THE STUN ALGORITHM FOR PERSISTENT SCATTERER INTERFEROMETRY

Bert M. Kampes, Nico Adam

German Aerospace Center (DLR) – Oberpfaffenhofen; 82234 Wessling, Germany; Bert.Kampes@dlr.de

ABSTRACT

The Spatio-Temporal Unwrapping Network (STUN) is a new algorithm to estimate displacement and topography at Persistent Scatterer (PS) points using an interferometric single-master data stack. The STUN algorithm provides a robust method to explicitly unwrap the interferometric phase using the temporal and spatial correlations of the observed phase. Moreover, it uses alternative hypothesis tests and the integer Least-Squares estimator to optimally estimate the parameters. Key features are the ability (i) to model the displacement using a linear combination of basefunctions; (ii) to estimate the precision of each SLC image using a novel stochastic model; (iii) to obtain a description of the precision of the estimated displacements.

This paper describes the STUN algorithm in detail, and demonstrates its practical application using data from a rural area nearby Marseille, France, which suffers from subsidence due to mining activities.

1   INTRODUCTION

The Spatio-Temporal Unwrapping Network (STUN) algorithm uses a displacement model and spatial network to unwrap the phase observations in a single-master stack of interferograms. It is a Persistent Scatterer Interferometry (PSI) processing algorithm, which originated from the description given in (Ferretti et al., 2000, 2001). The STUN algorithm uses the integer least-squares (ILS) estimator to unwrap the phase data temporally, and a minimal cost flow (MCF) sparse grid unwrapper to unwrap the data spatially. The precision of the estimated parameters is obtained by propogation of the precision of the phase observations, which is first estimated using a variance component estimation (VCE). The STUN algorithm is robust, because it uses the redundancy at the arcs of the spatial network to check for incorrectly estimated parameters using alternative hypotheses tests.

After unwrapping of the data, the topography and displacement parameters are estimated again. The residual phase at the PS points is filtered using Kriging interpolation to estimate the atmospheric signal. The products, topography and displacement at the PS points, are delivered in GeoTIFF format.

The key items of the STUN algorithm are explained in the first sections: Section 2 describes the functional and stochastic model, whereas section 3 describes the estimation of the parameters and the precision. The modular steps of the STUN algorithm are described in section 4 by means of a report of the processing performed in the framework of the PSIC4 study for ESA. Finally, conclusions are given in section 5.

2   MATHEMATICAL MODEL

The mathematical model comprises the functional model and the stochastic model, where the former defines the relationship between the observations and the unknown parameters, and the latter defines the variances of and covariances between the observations, see also (Teunissen, 2000a). At Delft University of Technology, a generic matrix notation is used to denote the mathematical model in the form of, possibly linearized, observation equations as

$$E\{\underline{y}\} = Ax, \qquad D\{\underline{y}\} = Q_y, \tag{1}$$

where $E\{\underline{y}\}$ is the expectation value of the observations $\underline{y}$ and $D\{\underline{y}\}$ denotes their dispersion. The underlining indicates a vector of stochastic variables. The design matrix A defines the functional relation between the observations $\underline{y}$ and the unknown parameters x. The dispersion of the observations is described by the variance-covariance matrix Q_y (vc-matrix). The mathematical model used in the STUN algorithm is described in more detail in (Kampes, 2005). Sections 2.1 and 2.2 briefly state the functional and stochastic model, respectively.

2.1 Functional Model

The functional model for PSI phase observations between two points is written using a partioned form of the left side of Eq. (1) as

$$\underline{y} = \begin{bmatrix} A|B \end{bmatrix} + \begin{bmatrix} a \\ b \end{bmatrix} + \underline{e} = Aa + Bb + \underline{e}, \tag{2}$$

where:

$\underline{y}$ is the vector of double-difference phase measurements, i.e., the phase differences between two points in a time series of interferograms.

a is the vector of integer-valued unknown ambiguities.

b is the vector of real-valued unknowns for the topography and displacement parameters.

A, B are the design matrices for the ambiguity terms and the parameters of interest, respectively.

$\underline{e}$ is the vector of measurement noise and unmodeled errors.

The observed wrapped phase differences are unwrapped as

$$\underline{\Phi}_x^k = \underline{\phi}_x^k + 2\pi \cdot a_x^k, \tag{3}$$

with integer ambiguity a_{xi}^k. The superscript k denotes the temporal phase difference between master and slave acquisition, and the subscript x the spatial phase difference between the phase at point x and some reference point. The observed phase lies in the principal interval $[-\pi, \pi)$, because only the fractional part of the returned carrier phase can be measured by the radar. It is our task to find the correct integer ambiguities a_x^k, because only the unwrapped phase difference can be related to the parameters of interest. The functional model for the unwrapped phase in interferogram k, corrected for the phase of a reference surface, is given as

$$\underline{\Phi}_x^k = \phi_{x,\text{topo}}^k + \phi_{x,\text{defo}}^k + \phi_{x,\text{atmo}}^k + \phi_{x,\text{orbit}}^k + \phi_{x,\text{noise}}^k. \tag{4}$$

The topographic phase is related to the difference in elevation Δh_x, between the point x and the reference point, as

$$\begin{aligned} \phi_{x,\text{topo}}^k &= -\frac{4\pi}{\lambda} \frac{B_{\perp x}^k}{r_x^m \sin\theta_{x,\text{inc}}^m} \cdot \Delta h_x \\ &= \beta_x^k \cdot \Delta h_x, \end{aligned} \tag{5}$$

where λ is the wavelength of the carrier signal used by the radar system, $B_{\perp x}^k$ is the local perpendicular baseline, r_x^m is the range from master sensor to the pixel, and $\theta_{x,\text{inc}}^m$ is the local incidence angle, see also (Rodriguez and Martin, 1992). The symbol β_x^k denotes the local height-to-phase conversion factor. It is assumed that the interferograms are corrected for the known topography using a DEM, and thus, the topographic term is related to the DEM error difference. However, it is also possible to use an ellipsoid model as reference surface, in which case the topographic term corresponds to ellipsoid height, if the reference point is located at the reference surface. Note that only topographic differences can be observed by radar interferometry (as well as displacement differences, atmospheric differences, etc.), and not the absolute values of these parameters.

The displacement term is caused by relative line-of-sight movement between the point x and the reference point, in the time between the acquisitions. It is equal to

$$\phi_{x,\text{defo}}^k = -\frac{4\pi}{\lambda} \Delta r_x^k, \tag{6}$$

where Δr_x^k is the line-of-sight displacement of x toward the radar since the acquisition time of the master image. In order to limit the number of parameters that needs to be estimated, the displacement behavior needs to be modeled and parameterized. Therefore, the displacement since the time of the master acquisition is modeled using a linear combination of base functions as

$$\Delta r_x^k = \sum_{d=1}^{D} \alpha_d(x) \cdot p_d(k). \tag{7}$$

For example, algebraic polynomials of the temporal baseline $T^k = t^0 - t^k$ (with t^0 and t^k the acquisition time of the master and slave, respectively) can be used

$$p_i(k) = (T^k)^i, \quad \text{for } i = 1, 2, \ldots \tag{8}$$

Finally, the atmospheric, orbit, and noise phase differences are lumped in a new random variable $\underline{e}$ with expectation $E\{\underline{e}\} = 0$. Thus, the functional model for the phase differences between two points is given by

$$E\{\underline{\Phi}_x^k\} = \beta_x^k \cdot \Delta h_x - \frac{4\pi}{\lambda} \sum_{d=1}^{D} \alpha_d(x) \cdot p_d(k). \tag{9}$$

In matrix notation this system of observation equations is written as in Eq. (2) as

$$E\left\{\begin{bmatrix} \underline{\phi}^1 \\ \underline{\phi}^2 \\ \vdots \\ \underline{\phi}^K \end{bmatrix}\right\} = \begin{bmatrix} -2\pi & & & \\ & -2\pi & & \\ & & \ddots & \\ & & & -2\pi \end{bmatrix} \begin{bmatrix} a^1 \\ a^2 \\ \vdots \\ a^K \end{bmatrix} + \begin{bmatrix} \beta_x^1 & p_1(1)..p_D(1) \\ \beta_x^2 & p_1(2)..p_D(2) \\ \vdots & \\ \beta_x^K & p_1(K)..p_D(K) \end{bmatrix} \begin{bmatrix} \Delta h \\ \alpha_1(x) \\ \vdots \\ \alpha_D(x) \end{bmatrix}. \tag{10}$$

For a linear displacement model, there is only one base function $p_1(k) = T^k$, and $\alpha_1(x)$ is the amplitude of the displacement rate difference between the points.

The number of double-difference observations is equal to the number of interferograms K. The number of unknown integer ambiguities is also equal to K, and the number of float parameters is, using a linear displacement model, $1 + D = 2$. Because there are more unknown parameters than observations, this is an under-determined system of equations with an infinite number of solutions. To solve it, additional constraints have to be introduced. This regularization is described in section 3.1.

2.2 Stochastic Model

The stochastic model describes the dispersion of the time series of double-difference phase observations. A variance components model is derived in (Kampes, 2005) for these observations in a single-master stack as

$$Q_{\text{ifg}} = \sum_{k=0}^{K} \sigma_{\text{noise}^k}^2 Q_k, \quad \text{where } Q_k = \begin{cases} 2E_K & \text{if } k = 0 \text{ (master)} \\ 2i_k i_k{}^* & \text{if } k = 1, \dots, K \end{cases}. \tag{11}$$

Here, the vc-matrix of the double-difference observations is written as a variance component model, using $K+1$ cofactor matrices Q_k and $K+1$ variance components $\sigma_{\text{noise}^k}^2$. Matrix E_K is a $K \times K$ matrix filled with ones, and i_k is a $K \times 1$ vector with a single one at position k (the asterisk denotes the transposition). It is assumed that all points in an interferogram have the same inherent noise level $\sigma_{\text{noise}^k}^2$, and that the noise is uncorrelated between the various SLC images. In (Kampes, 2005) it is shown that the variance components actually describe $\sigma_{\text{noise}^k}^2 + \sigma_{\text{atmo}^k}^2(0) - \sigma_{\text{atmo}^k}(l)$, i.e., they are actually also related to the variance of the atmospheric difference signal between points at a distance l apart. Section 3.3 describes how the variance components can be iteratively estimated.

For example, if the inherent noise σ_{noise}^2 would be equal for all acquisitions, and if mis-registration causes an equal additional amount of noise in the slave images, the vc-matrix Q_{ifg} for the double-difference observations becomes

$$Q_{\text{ifg}} = \sigma_{\text{noise}}^2 \begin{bmatrix} 6 & 2 & 2 & 2 & \dots & 2 \\ 2 & 6 & 2 & 2 & \dots & 2 \\ \vdots & & \ddots & & & \\ & & & & & \\ & & & & & \\ 2 & 2 & 2 & \dots & 2 & 6 \end{bmatrix}. \tag{12}$$

From Eq. (12) it can be clearly seen that the time series of the double-differenced observations are correlated.

3 PARAMETER ESTIMATION

In the STUN algorithm, the integer least-squares adjustement is used to estimate the unknown integer ambiguities and the float parameters, e.g., the DEM error and the displacement rate. The system of equations Eq. (10) needs to be regularized before the estimation, because it is under-determined. The variance components are estimated using a variance component estimation following an initial estimation using an a priori model. The estimated stochastic model is used during the final estimation of all points. The following sections describe these issues in more detail.

3.1 Regularization of the System of Equations

The system of equations Eq. (10) is under-determined and cannot be solved without introducing additional constraints. Note that such constraints are also used during conventional spatial phase unwrapping, because the observed wrapped phase values at the pixels of the interferogram are not correlated, i.e., each pixel can have a random ambiguity, which in itself is as likely as any other. It is assumed that the topography and/or the displacement are spatially correlated (this is the additional constraint), and the ambiguities are estimated such that this spatial correlation is best reflected.

For the problem at hand, regularization of Eq. (10) is achieved as in (Bianchi, 2003; Hanssen et al., 2001), by adding zero pseudo-observations $\underline{y}_2$ with some uncertainty described by Q_{y_2}

$$E\{\begin{bmatrix} \underline{y}_1 \\ \underline{y}_2 \end{bmatrix}\} = \begin{bmatrix} A_1 \\ A_2 \end{bmatrix} a + \begin{bmatrix} B_1 \\ B_2 \end{bmatrix} b, \qquad D\{\begin{bmatrix} \underline{y}_1 \\ \underline{y}_2 \end{bmatrix}\} = \begin{bmatrix} Q_{y_1} & 0 \\ 0 & Q_{y_2} \end{bmatrix}. \tag{13}$$

Matrices $\underline{y}_1$, A_1, and B_1 are defined in Eq. (10). A_2 is a zero matrix $O_{D+3 \times K}$, and B_2 is an identity matrix I_{D+3}. The value of the pseudo-observations is chosen as $\underline{y}_2 = 0$. Matrix Q_{y_2} is a diagonal matrix that describes the uncertainty of the unknown parameters. The dispersion of the pseudo-observations follows from an appropriate (pessimistically chosen) a priori standard deviation of the unknown parameters. Reasonable values are for example $\sigma = 20$ m for the DEM error difference, $\sigma = 20$ mm/y for the linear displacement rate difference. The dispersion of the pseudo-observations serve as "soft"-bounds to limit the search space that is sought to find a solution for the integer and float parameters. This augmented system of equations is again written symbolically similar to Eq. (1) as

$$E\{\underline{y}\} = Aa + Bb, \qquad D\{\underline{y}\} = Q_y. \tag{14}$$

3.2 Integer Least-Squares Estimation

The basic task is to estimate the K integer ambiguities and the $1 + D = 2$ real-valued parameters from the K observed wrapped phase values. Since the estimation criterion is based on the principle of least-squares, the estimates for the unknown parameters of Eq. (2) follow from solving the minimization problem

$$\min_{a,b} \|\underline{y} - Aa - Bb\|_{Q_y}^2 \quad \text{subject to } a \in \mathbb{Z}, \ b \in \mathbb{R}, \tag{15}$$

where $\|.\|_{Q_y}^2 = (.)^* Q_y^{-1}(.)$ and Q_y is the vc-matrix of the observables. This minimization problem is referred to as an integer least-squares problem in (Teunissen, 1994). It is a constrained least-squares problem due to the integer constraint $a \in \mathbb{Z}$. It is the best possible estimator, in the sense that it gives the highest probability of correct integer estimation (ambiguity success rate) for problems with a multivariate normal distribution, see (Teunissen et al., 1995).

Using the Least-squares AMBiguity Decorrelation Adjustment (LAMBDA) method, the solution for the integer ambiguities is found in three steps, see also (Kampes, 2005; Kampes and Hanssen, 2004; Teunissen, 1995)

1. Transform the problem using a decorrelation, such that the solution can be found faster.
2. Compute the "float solution" for the unconstrained, transformed, problem, i.e., ignoring the fact that the ambiguities are integers.
3. Search the solution space of the integer ambiguities based on the "float solution" to find the "fixed solution". An efficient sequential conditional least-squares search is performed, until the solution is found that satisfies Eq. (15). Note that no direct inversion exists for this problem and that this method searches the ambiguity solution space, not that of the float parameters. This makes it very easy to extend the functional model for more complicated displacement models, without increase of computation time.

The found set of integer ambiguities of step 3 are back-transformed to the original parameterization using an inverse transformation. These ambiguities are used to unwrap the observed data, which are then used to estimate the float parameters for the DEM error and displacement.

The LAMBDA method was developed for fast ambiguity resolution of GPS carrier phase measurements. Free software is distributed by Delft University of Technology that implements this method, see (Delft University of Technology, 2005).

3.3 Variance Components Estimation

If the variance components in Eq. (11) are assumed to be unknown, a variance component estimation technique can be used to obtain estimates for them. An initial estimation of the unknown parameters is required before estimation of the variance components is possible. During this initial estimation, a stochastic model with a priori variance components[1]

---

[1] $\sigma_{\text{noise}0}^2 = (20°)^2$, and $\sigma_{\text{noise}k}^2 = (30°)^2$ for $k = 1, \ldots, K$

is used cf. Eq. (11). This a priori model is based on the assumptions that the interferometric phase standard deviation for point scatterers is expected to be below ~50°, and that slight mis-registration introduces a small amount of additional noise in the slave images. Note that the variance component estimation can be performed iteratively, and that the choice of the stochastic model during the initial estimation is not very important, e.g., a scaled identity matrix $\sigma_{\mathrm{noise}}^2 I_K$ could also be used, initially. The vector of variance components of the SLC images $\sigma = [\sigma_{\mathrm{noise}^0}^2, \ldots, \sigma_{\mathrm{noise}^K}^2]^*$ is estimated by using the temporal least-squares interferometric phase residuals vector $\underline{\hat{e}}$ of the initial estimation between two points as (Verhoef, 1997)

$$\underline{\hat{\sigma}} = N^{-1}\underline{r}, \tag{16}$$

where N is a square $(K{+}1){\times}(K{+}1)$ matrix. The elements of these matrices are given by

$$\underline{r}(k{+}1) = \underline{\hat{e}}^* Q_y^{-1} Q_k Q_y^{-1} \underline{\hat{e}},$$
$$N(k{+}1, l{+}1) = \mathrm{trace}(Q_y^{-1} P_B^\perp Q_k Q_y^{-1} P_B^\perp Q_l), \tag{17}$$

for $k, l = 0, \ldots, K$ (Q_k is defined in Eq. (11)). The least-squares orthogonal projection matrix $P_B^\perp$ is given by $P_B^\perp = I_K - B(B^* Q_y^{-1} B)^{-1} B^* Q_y^{-1}$. The vc-matrix of the estimated variance components is given by (Verhoef, 1997)

$$D\{\underline{\hat{\sigma}}\} = 2N^{-1}. \tag{18}$$

This variance is reduced by using more estimations between points. If each point in these estimations is used only once (see for an example Fig. 2(a)) the estimate for the variance components corresponding to the parameterization (11) is given by the mean of these estimations. If all arcs have a similar length, then the mean variance components account for the inherent noise at the points and the typical atmospheric difference signal between points, say, 1 km apart, during the SLC acquisition. The variance of the estimated variance components is reduced by the number of estimations. In order to supress the variance of the estimated variance components to a reasonable level, at least a few hundred arcs should be used.

4   REAL DATA PROCESSING

The PSIC4 Study (Persistent Scatterer Interferometry Codes Cross-Comparison and Certification for long term differential interferometry) was initiated by ESA following a recommendation made during the Fringe 2003 Workshop to assess the reliability and dependability of PSI methods. It had a duration of six months, starting in December, 2004. Several international teams processed the same data of ERS and ENVISAT imagery using their PSI processing systems. The results are evaluated and compared by an independent validation consortium using ground truth displacement data.

The following sections present a report of the processing performed at DLR using the STUN algorithm in the framework of this study. This provides an overview of all the processing steps, which are briefly introduced at the beginning of each section.

4.1   Generation of the single-master stack

The interferograms are generated after calibration and oversampling of the data. Coregistration of the slave images is performed using a robust algorithm that uses the orbit geometry and a DEM of the area, and using the precisely estimated sub-pixel position of identified point scatterers distributed over the image, see also (Adam et al., 2003).

For the estimation, 79 ERS scenes were used, acquired between 1992 and 2004. The master image is orbit 20460 (ERS-2), acquired at March 20, 1999. This acquisition is selected because the results need to be delivered with respect to this image for this study. The perpendicular baselines are between -1150 m and 950 m, and the maximum Doppler centroid frequency difference is 700 Hz. The processed area is $2392{\times}19380$ oversampled pixels (range, azimuth), approximately $24{\times}40$ km^2, using a ground-range pixel posting of 10 meters and azimuth resolution of 2 meters. The SRTM C-Band DEM, converted from geoid height to ellipsoid heights, is used for the topographic correction. Fig. 1 shows a topographic map and the average intensity map of the processed area, as well as an example differential interferogram with favorable, small, perpendicular and temporal baselines. Note that this interferogram is decorrelated to a large extend, particularly in the rural and mountainess area.

After creation of the stack, PS points are selected based on an approximate Signal-to-Clutter Ratio (SCR). This SCR is defined as the ratio of the power of the considered pixel with its immediate neighboring pixels. For the PSIC4 study, points were selected for which this value was larger than 2.0, which selected 161116 of ~50 million image pixels in the
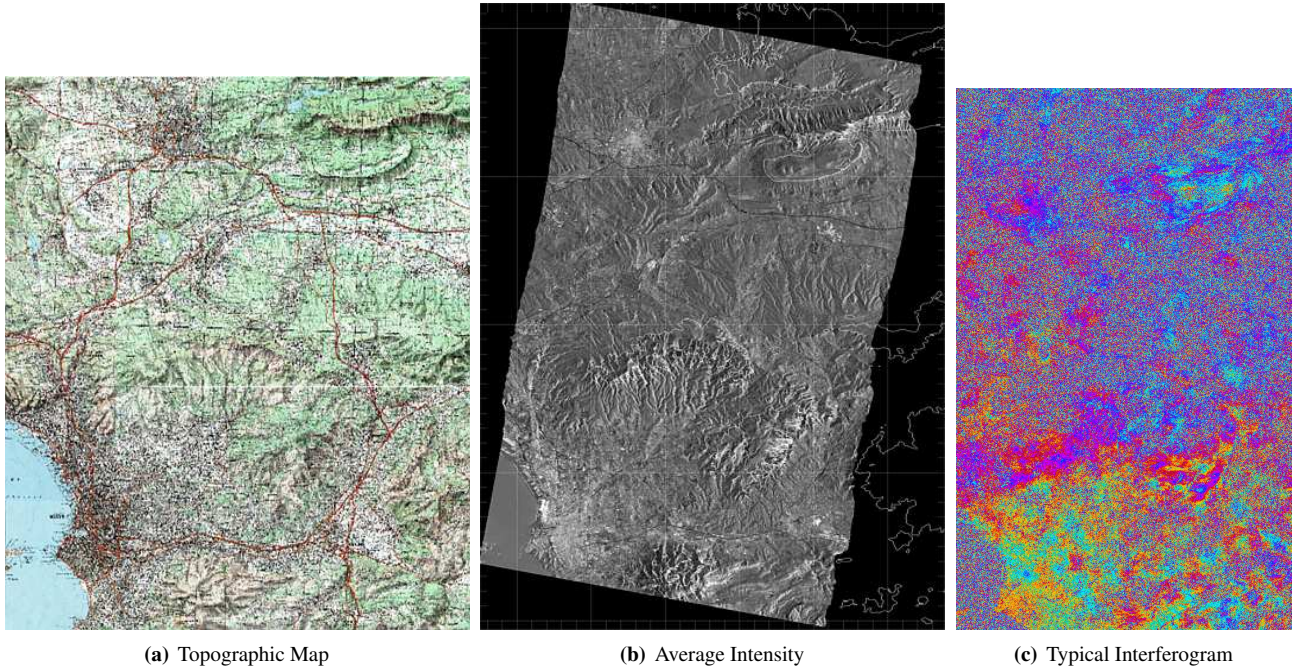
(a) Topographic Map   **(b)** Average Intensity   **(c)** Typical Interferogram

Figure 1: Topographic map, average radar intensity (geocoded), and typical interferogram (orbit 24969, $B_\perp = -120$ m, $T = 315$ days) for the processed area near Marseille, France.

oversampled data (0.35%). For each of these pixels, a point target analysis (PTA) is performed, and the peak position and phase at this position are extracted. Points that are not selected are discarded for further processing. The main advantage of discarding more than 99 percent of the data is a reduction of the computing time.

4.2   PSIC4 Variance Components Estimation

The first step of the STUN algorithm is to estimate the precision of the phase observations using a variance component estimation. As described in section 3.3, this estimation is performed following an initial estimation of the parameters at independent arcs of approximately the same length. Fig. 2 shows the arcs used during the VCE, and the average of the estimated variance factors at these arcs, computed by Eq. (16).
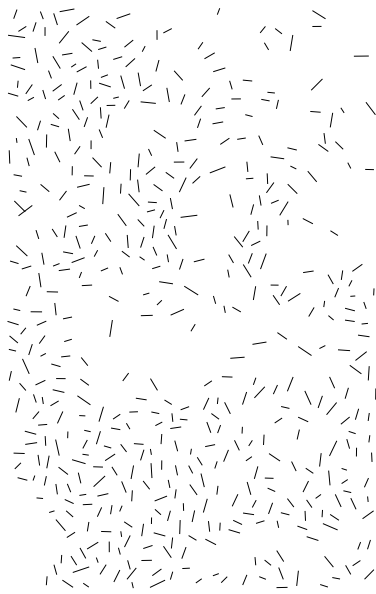
Performing a VCE improves the quality of the estimated parameters, due to more realisitic weighting, reduces the number of incorrectly estimated ambiguities during the non-linear inversion using the ILS, and is a way to automatically detect incorrectly processed interferograms. Moreover, it is possible to obtain a realistic description of the precision of the estimated parameters.
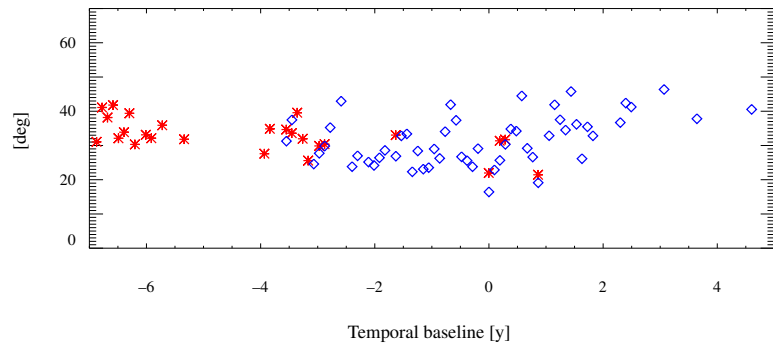
4.3   Reference Network Computation

The selected points, based on the SCR, are divided in two groups: reference network points and other points. The reference network points are expected to are most phase stable, based on their amplitude dispersion index (Ferretti et al., 2001). The DEM error and the displacement rate are estimated at all arcs of this reference network. This network is created such that each point has many connections to nearby points, which is done to enable detection of arcs and/or points that are estimated incorrectly. Fig. 3 shows the selected points and the reference network.

Integration of Estimated Difference Parameters

The parameters DEM error and displacement rate (assuming this base function) can be obtained by integration of the estimated DEM error differences and displacement rate differences at the arcs of the network. The DEM error at the points can be obtained with respect to the reference point (the first point; i.e., this unknown is removed from the vector of unknown parameter together with the corresponding column of the design matrix) by solving a system of observation
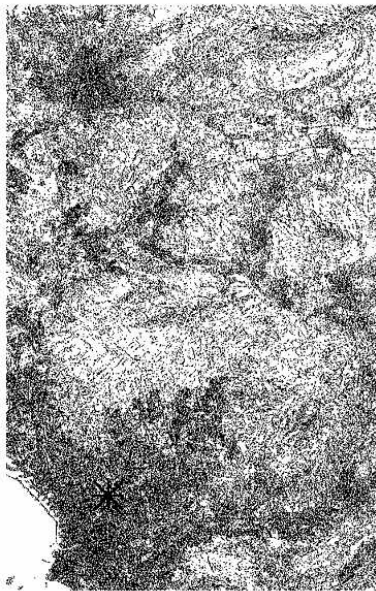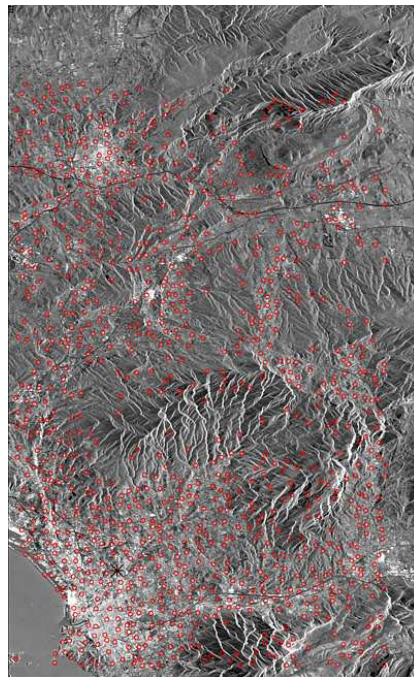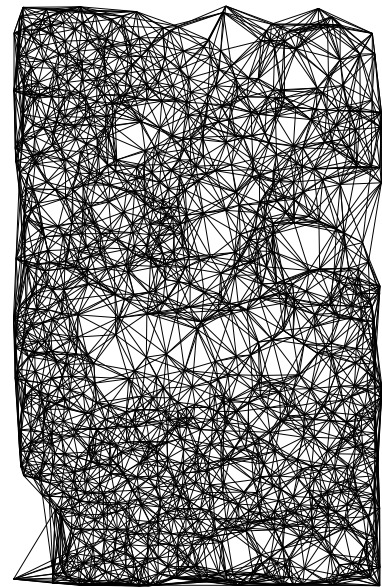
(a) Arcs for VCE

(b) Variance Components

Figure 2: Variance component estimation. The components are estimated independently at each arc shown in **(a)**. The number of arcs is 507, with a mean length of 620 m. The mean of these estimates is shown in **(b)**, which indicates the average precision of the master and co-registered SLC images. Plotted are the square roots of the factors, sorted according to temporal baseline. N arcs, mean length=X; what is this... the standard deviation of the phase noise at a point, and it includes the due to

(a) Selected Points   (b) Reference Network Points   (c) Reference Network

Figure 3: Selected points. The left panel shows all selected points that are analyzed, having an SCR<2. The middle panel shows the points with the smallest amplitude dispersion index in each cell of 500×500 m^2, which are expected to possess a stable phase behavior in time. The right panel shows the reference network. At the arcs of this network the DEM error difference and displacement rate difference are estimated using the ILS estimator. The network contains 1047 points and 6674 arcs, i.e., 12.7 connections per point. The mean arc length is 1280 m, with a standard deviation of 646 m.
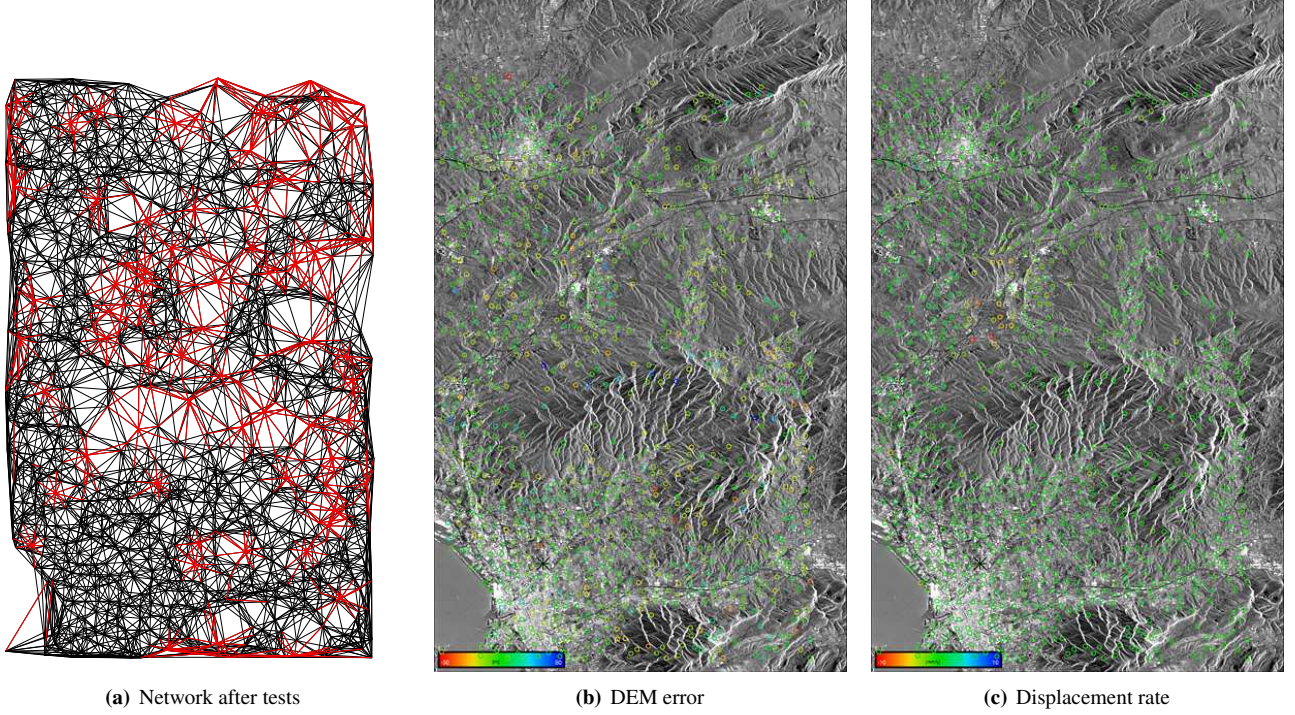
(a) Network after tests   **(b)** DEM error   **(c)** Displacement rate

Figure 4: Estimated parameters at the accepted points of the reference network. The left panel shows the network after the hypothesis tests. Estimated parameters at the red arcs are rejected during an iterative procedure, based on the adjusted least-squares residual at the arcs. The middle panel shows the integrated DEM error at the reference network points, relative to the selected reference point (asterisk), for which the DEM error is assumed to be zero. The right panel shows the estimated displacement rates, also relative to the selected reference point.

equations like

$$
\begin{bmatrix}
\Delta h_{2,1} \\
\Delta h_{3,1} \\
\Delta h_{4,1} \\
\vdots \\
\Delta h_{3,2} \\
\Delta h_{4,2} \\
\vdots \\
\Delta h_{H-1,H}
\end{bmatrix}
=
\begin{bmatrix}
-1 & 0 & 0 & \ldots & & 0 \\
0 & -1 & 0 & \ldots & & 0 \\
0 & 0 & -1 & \ldots & & 0 \\
\vdots & & & & & \\
1 & -1 & 0 & \ldots & & 0 \\
1 & 0 & -1 & \ldots & & 0 \\
\vdots & & & & & \\
0 & 0 & 0 & \ldots & 1 & -1
\end{bmatrix}
\begin{bmatrix}
\Delta h_2 \\
\Delta h_3 \\
\Delta h_4 \\
\vdots \\
\Delta h_{H-1} \\
\Delta h_H
\end{bmatrix},
\tag{19}
$$

where the observations on the left hand side are the estimated DEM error differences at the arcs, the design matrix C on the right hand side corresponds to the estimated arcs, and the vector on the left contains the unknown DEM error at the points. The solution for the unknown parameters $\hat{\underline{b}}$ is given by the well-known least-squares formulas

$$
\begin{aligned}
Q_{\hat{b}} &= (C^* Q_y^{-1} C)^{-1}, & Q_{\hat{y}} &= C Q_{\hat{b}} C^*, & Q_{\hat{e}} &= Q_y - Q_{\hat{y}}, \\
\hat{\underline{b}} &= Q_{\hat{b}} C^* Q_y^{-1} \underline{y}, & \hat{\underline{y}} &= C \hat{\underline{b}}, & \hat{\underline{e}} &= \underline{y} - \hat{\underline{y}},
\end{aligned}
\tag{20}
$$

where $Q_{\hat{b}}$ is the estimated vc-matrix for the unknowns (DEM error), $Q_{\hat{y}}$ that of the adjusted observations, $Q_{\hat{e}}$ that of the least-squares residuals, and $\hat{\underline{b}}$, $\hat{y}$, and $\hat{\underline{e}}$ are the vectors of adjusted unknowns, observations and residuals, respectively. An identical design matrix is used to "integrate" the other estimated difference parameters independently, in this example the displacement rate differences at the arcs.

This system of equations looks very similar to that of a leveling network. However, the difference is that here the least-squares residuals (the misclosures) at the arcs must be exactly zero, because there are no actual observations between points, which, on the contrary, is the case with leveling data. If all spatial residuals are indeed equal to zero, the least-squares estimates at the points are the same as those that would be obtained after integration along any path.
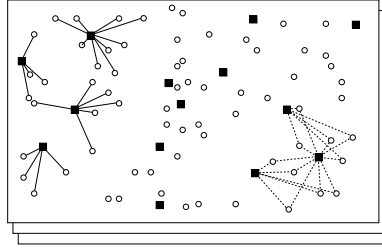
Figure 5: Connection of new points (circles) to the reference network pixels (squares). Each selected point is connected to the nearest point in the reference network, and a relative estimation is performed using the integer least-squares estimator. These connections are indicated at the left hand side of this figure. Alternatively, each new point can be connected to a couple of points of the reference network, indicated at the right hand side.

Alternative Hypothesis Tests

The integrity of the network should be checked, because it is possible that the estimated parameters at the arcs are not correct. This can occur when a point is not coherent, or when the incorrect set of ambiguities is estimated that better fits the data due to noise. Note again that the situation for the created network is not the same as for, e.g., a leveling network Here, the misclosures must be perfectly zero, because there is no independent measurement (noise) on the arcs. A misclosure is solely due to incorrectly estimated parameters at an arc. Such an error should not be adjusted, but the cause must be found and rectified. Moreover, the network testing procedure does not have to be approached as strict as for, e.g., a leveling network. After all, if the misclosure is zero, removing a (correctly estimated) arc does not change the parameter solution or its precision. However, zero misclosures do not guarantee that the parameters are estimated correctly (they can all be consistently incorrect), but it does mean that all errors that could be found are dealt with.

In order to find outlier arcs and points, an alternative hypotheses testing strategy is used, known as DIA procedure (Teunissen, 2000b). First, in the *detection* step, the null-hypothesis is tested against general model mis-specifications. If this test is rejected alternative hypotheses are specified to *identify* the most likely cause. Alternative hypotheses are specified to detect outlier arcs and outlier points. In the *adaption* step, the functional model is changed to account for the identified cause, i.e., an arc or a point is removed from the system of equations. These steps are repeated until the null-hypothesis is accepted. See also (Kampes, 2005). Fig. 4 shows the network after the hypothesis tests and the integrated DEM error and displacement rates at the points.

4.4 Estimation of all selected points

Once the reference network is established and the DEM error and displacement parameters at the points in the reference network are computed and tested, the other ~100000 points that were initially selected can be estimated. This estimation is again performed with the integer least-squares estimator, identically to the estimation at the arcs of the reference network. Each new point is connected to the nearest point of the reference network and the wrapped phase difference time series is used to estimate the DEM error and displacement parameters differences between the reference point and the new point, see also Fig. 5. The parameters of the reference points are considered to be deterministic at this moment, which implies that the parameters of the new points are simply given by addition. The distance of the newly computed points to the points of the reference network is smaller than the typical distance between the points of the reference network. The atmospheric phase is thus also expected to be smaller. However, the random noise component is likely larger for the new points, since the reference network points were selected as the points with the smallest amplitude dispersion index. The same vc-matrix of Eq. (11) and estimated variance components are used during this estimation. The functional model is given in, e.g., Eq. (10), where integer ambiguities, DEM error, displacement rate, and azimuth sub-pixel position are estimated. To deselect incoherent points, an a posteriori variance factor is estimated for each arc (point) as

$$\hat{\underline{\sigma}}_x^2 = \frac{\hat{\underline{e}}^* Q_y^{-1} \hat{\underline{e}}}{r}, \tag{21}$$

where $\hat{\underline{e}}$ are the temporal least-squares residual phase (differences) vector, and r is the redundancy (i.e., the number of interferograms minus the number of estimated parameters). An estimated variance factor of 1.0 signifies that the vc-matrix used during the least-squares adjustment correctly describes the dispersion of the observations, while a value of 2.0 would signify that the stochastic model is a factor two too optimistic (assuming that the functional model is correct). These a posteriori variance factors thus scale for each point the estimated components of the variance components stochastic model, given in Eq. (11).
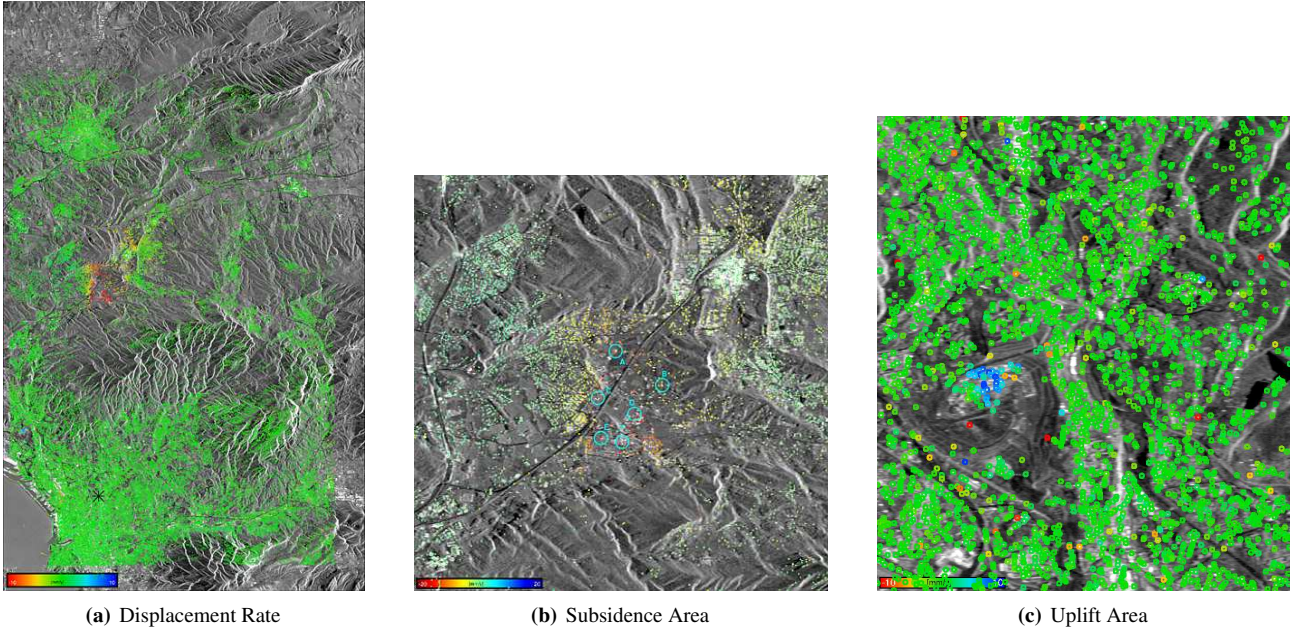
(a) Displacement Rate   **(b)** Subsidence Area   **(c)** Uplift Area

Figure 6: Estimated displacement rates. A zoom of the central subsidence area near the city of Gardanne is shown in **(b)**, as well as a zoom of an uplift area slightly North of Marseille in **(c)**. Time series of the indicated points are given in Fig. 7.

4.5 Spatial phase unwrapping

In the STUN algorithm, an explicit unwrapping of the phase data is performed. This step follows after the inclusion of more points, described in the previous section. Only points that have a small residual phase with respect to the (temporal) model are used for the spatial unwrapping. The reason is that points that are incorrectly unwrapped in time can hardly be distinguished from correctly estimated points after addition of the unwrapped residual fields, since the temporal least-squares residuals are $\in [-\pi, \pi)$. by definition, while the spatially unwrapped residuals can be considerably larger due to, e.g., atmospheric artifacts. For example, consider a point that is fully coherent (and which does not undergo displacement), far away from the reference point, and a point that is fully incoherent, near to the reference point. Both points are temporally unwrapped by the ILS estimator with respect to a coherent reference pixel. The parameters that are estimated for the incoherent point are random, but they do minimize a norm with respect to the model. The wrapped residual phase differences of Eq. (21) are much smaller for the coherent point, as is the estimated variance factor. However, after the spatial unwrapping process, the unwrapped residuals at the incoherent point could be smaller due to its proximity to the reference point (and consequently the smaller expected atmospheric phase). Therefore, only pixels with an a posteriori variance factor, cf. Eq. (21), below a certain threshold k are included in the spatial unwrapping,

$$\hat{\underline{\sigma}}_x^2 < k, \tag{22}$$

with, for example, $k{=}2.0$. The value of this threshold depends on the vc-matrix used during the ILS estimation, since the estimated variance factor is a multiplication factor for this matrix.

After that the parameters are estimated, the unwrapped model phase can be computed for each point in all interferograms, using the forward model, as

$$\hat{\underline{\Phi}}_x = B\hat{\underline{b}}_x. \tag{23}$$

Since the observed phase is wrapped, only the wrapped residual phase is obtained, i.e.,

$$W\{\hat{\underline{e}}_x\} = W\{\underline{\phi}_x - \hat{\underline{\Phi}}_x\}. \tag{24}$$

The residual phase at the selected points in each interferogram are expected to contain a low-frequency component caused by interferometric atmospheric signal and possible unmodeled displacement, and a small amplitude, high-frequency component due to random noise. This property can be exploited by application of a spatial complex low-pass filter to the wrapped residuals. The residual phase per interferogram can then first be demodulated for the low-pass component, which can then be unwrapped separately from the high-pass component. The total unwrapped field is given by addition
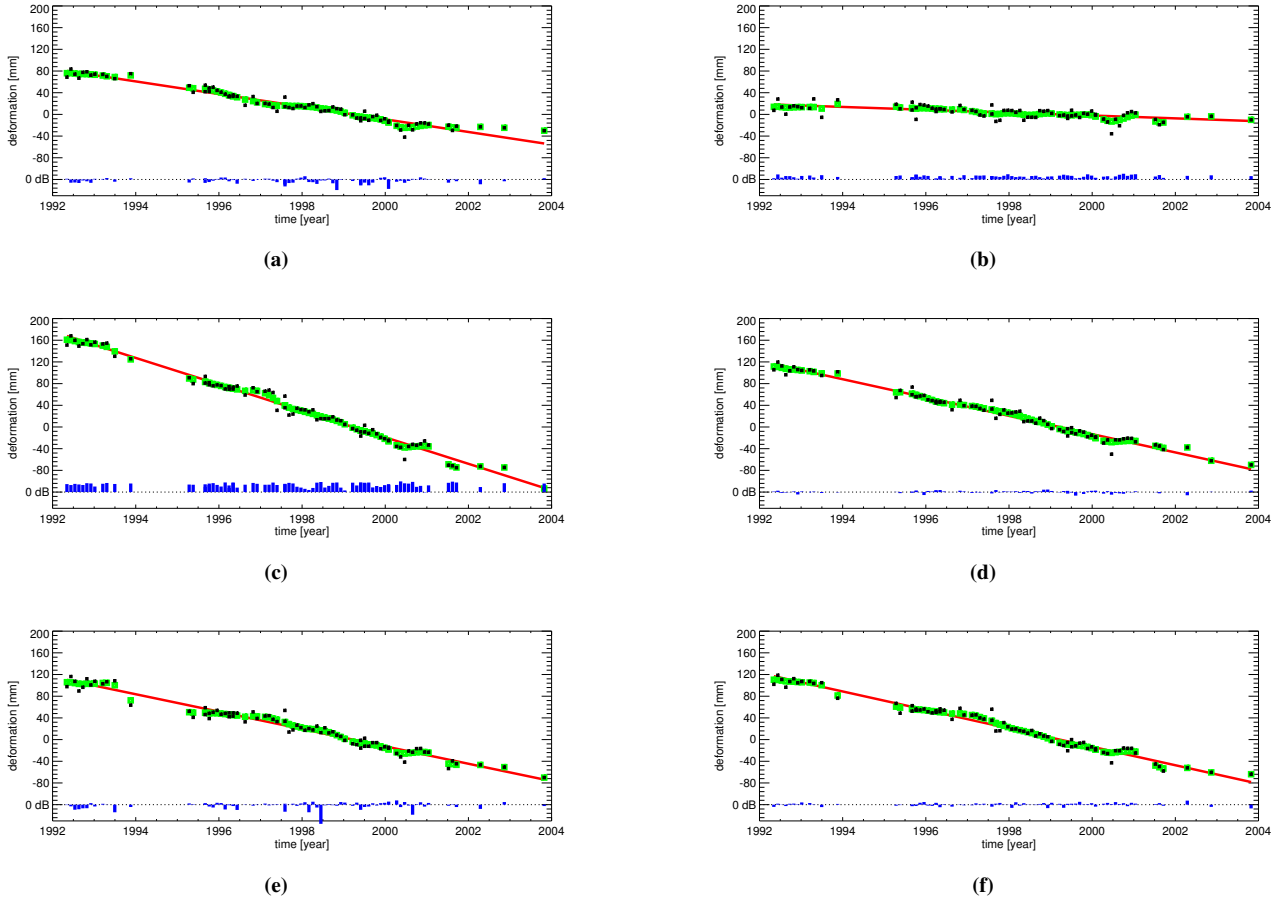
Figure 7: Time series for points in the subsidence area, see also Fig. 6(b). The black squares show the unwrapped data, the green correspond to the temporal low-pass filtered using a triangular window with length 1 year. Data are not prior corrected for atmospheric signal. The red lines show the estimated average displacement rate. The amplitude is indicates at the bottom in decibel. The panels correspond to the six points indicated in the subsidence area, for which the average displacement rates are A: -11.7, B: -2.6, C: -24.4, D: -16.9, E: -16.0, F: -17.0 mm/y, respectively.

of the two unwrapped components. However, to unwrap the residual fields for each interferogram, a sparse grid MCF unwrapping algorithm (Eineder and Holzner, 1999) is directly applied in our implementation. The distance between the points is used to generate the cost function. Once the residual fields are unwrapped, the unwrapped phase at the selected point is obtained by addition of the unwrapped residual phase $\check{\underline{e}}_x$ to the model phase

$$\check{\underline{\Phi}}_x = \hat{\check{\underline{\Phi}}}_x + \check{\underline{e}}_x. \tag{25}$$

The unwrapped phase at a reference point must be set to zero in all interferograms. This reference point does not have to be identical to the previously selected one. However, it must be a point that has a relatively small noise component in all interferograms, i.e., the reference point must be present during all acquisitions.

Non-linear Displacement Temporal Filter

After spatial phase unwrapping, the parameters are again estimated, now using the unwrapped data. The unwrapped least-squares residuals are automatically obtained after this estimation. If it is assumed that the displacement model does not fully describe the actual displacement, additional base functions can be defined that better describe it. For example, piecewise polynomials could be used, or polynomials of a higher degree.

Alternative, a temporal filter can be used to filter temporally correlated signal from the unwrapped residuals. In this approach it is assumed that the atmospheric signal is uncorrelated in time, while the displacement signal is correlated. Fig. 7 shows for six points in the subsidence area the unwrapped phase, the estimated linear displacement rate, and a temporally low-pass filtered version using a triangular window with a length of 1 year. Note that there may be unwrapping
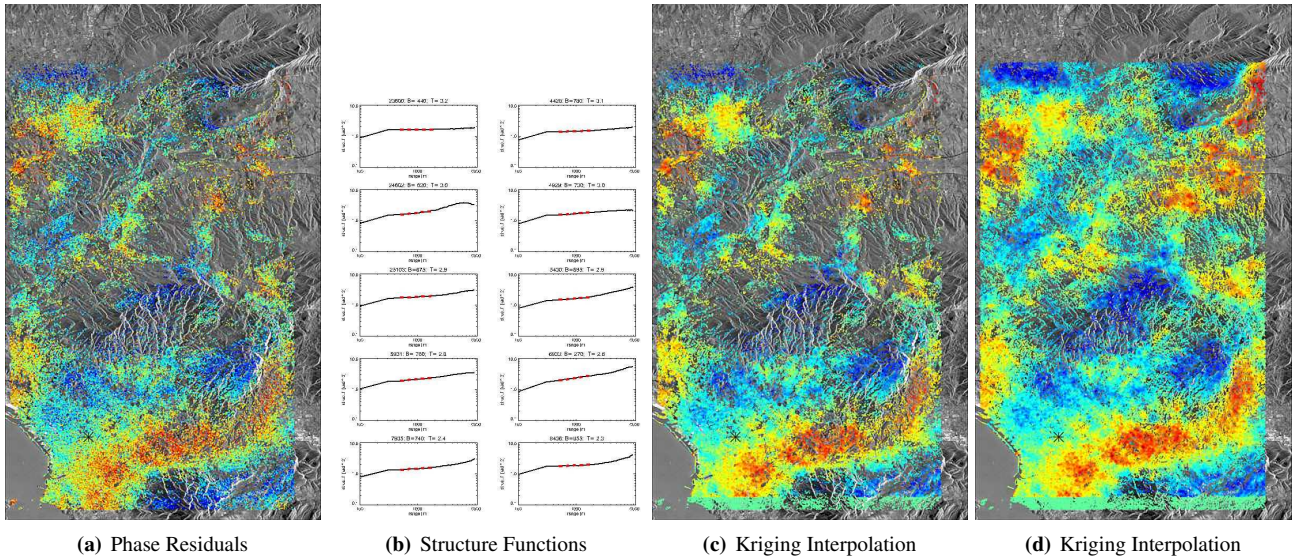
(a) Phase Residuals   **(b)** Structure Functions   **(c)** Kriging Interpolation   **(d)** Kriging Interpolation

Figure 8: Kringing interpolation. The left panel shows the residual interferometric phase for interferogram with slave orbit 24602 ($B_\perp = -620$ m, $T = -3.0$ y). at approximately 60000 accepted points. **(b)** shows the structure functions computed for a number of interferograms in a loglog plot. The expected slope of the structure functions is indicate by the dotted lines in the background. The dashed line shows the estimated slope in the interval between 500 and 2500 meter, which is used as input for the Kriging Interpolation using a power-law model. The structure function for interferogram 24602 is shown in the left panel of the second row. The slope of this interferogram is 0.22, i.e., significante less than the expected 0.67 for atmospheric signal at these distances. In general, the estimated slopes are between 0.1 and 0.3, which may indicate that other signal is present in the residual phase aside from atmospheric signal, or that the power of the noise is higher than the power of the atmospheric signal. **(c)** shows the Kriging result at the original points, and **(d)** shows the interpolation at all selected points. All data are plotted in the range $[-\pi, \pi]$ rad.

errors in these data. Particularly visible in Fig. 7(e) is that due to linear displacement model the earlier acquisitions lie on the red line, whereas maybe these data should be one or two wraps lower (28 or 56 mm). The same is valid for the later data after the year 2000.

Atmospheric Signal Spatial Filter

As noted in the previous section, the unwrapped phase residuals contain random noise, atmospheric signal, and displacement signal that is not modeled. For the PSIC4 study, it is assumed that the linear displacement model correctly describes the actual displacements. Therefore, the atmospheric signal can be obtained directly using Kriging interpolation of the residuals, i.e., a temporal filter is not applied. Fig. 8 shows the Kriging interpolation for an interferogram with relative large amount of atmospheric signal. The spatially low-pass filtered residual phase is subtracted from the time series in the delivered result. Note that in the STUN algorithm it is not necessary to estimate the atmospheric signal, because the unwrapped phase is obtained at all points beforehand.

4.6 Geocoding

ESA provided the ellipoid coordinates (WGS84) of five Ground Control Points (GCPs) to enable an accurate geocoding of the delivered PS points. The approach followed to make use of these points was to split up the problem in a horizontal and vertical problem. First, the timing of the master acquisition is calibrated. For this reason, the GCPs are located in the average intensity map, which is in the master geometry. The GCPs could be located within a few image pixels, because they were, for example, the crossing of major roads. The annotated azimuth and range timing were then corrected such that the radarcoded (inversely geo-referenced) GCP positions matched best, in a least-squares sense, with the measured positions in the average intensity map.

Second, the height of the reference point needs to be determined. For this reason, the estimated heights of the five PS points closest to a GCP is averaged, and an average offset is determined for all GCPs. This height offset is added to the estimated heights at all PS points.

The estimated DEM error, displacement rates and timeseries are delivered in GeoTIFF format. Fig. 9 shows the geo-reference points on top of a aerial photograph of the area.

Figure 9: Data plotted on top of an aerial photo (obtained via maps.google.com). No correction is made to shift the background image such that it aligns best with the geo-referenced displacement rates. This image illustrates the point density in the subsidence area and possibilities of GIS/geoTIFF interface.

5 CONCLUSIONS

A new Persistent Scatterer processing algorithm is presented, as well as a processing example using real data in a rural area. The key elements of this algorithm are that the precisions of the radar observations are estimated using a variance component estimation, and that this stochastic model is used during estimation of the parameters for topography and displacement. For this estimation, the integer least-squares is proposed. The data are unwrapped using a minimal costflow algorithm on a sparse grid. Temporal and spatial filtering of the unwrapped data is performed to isolate atmospheric signal, noise and unmodeled displacement signal.

6 REFERENCES

References

Adam, N., Kampes, B. M., Eineder, M., Worawattanamateekul, J. and Kircher, M.: 2003. The development of a scientific permanent scatterer system. *ISPRS Workshop High Resolution Mapping from Space, Hannover, Germany, 2003*. pp. 1–6 (cdrom).

Bianchi, M.: 2003. *Phase ambiguity estimation on permanent scatterers in SAR interferometry: the integer least-squares approach*. Master's thesis. Politecnico di Milano/Delft University of Technology.

Delft University of Technology: 2005. Mathematical Geodesy and Positioning web page. `http://enterprise.lr.tudelft.nl/mgp/` (Accessed April, 2005).

Eineder, M. and Holzner, J.: 1999. Phase unwrapping of low coherence differential interferograms. *International Geoscience and Remote Sensing Symposium,* Hamburg, Germany, 28 June–2 July, 1999. pp. 1–4 (cdrom).

Ferretti, A., Prati, C. and Rocca, F.: 2000. Process for radar measurements of the movement of city areas and landsliding zones. International Application Published under the Patent Cooperation Treaty (PCT).

Ferretti, A., Prati, C. and Rocca, F. 2001. Permanent scatterers in SAR interferometry. *IEEE Transactions on Geoscience and Remote Sensing* 39(1), 8–20.

Hanssen, R. F., Teunissen, P. J. G. and Joosten, P.: 2001. Phase ambiguity resolution for stacked radar interferometric data. *International Symposium on Kinematic Systems in Geodesy,* Geomatics and Navigation, Banff, Canada, 5–8 June, 2001. pp. 317–320.

Kampes, B. M.: 2005. *Displacement Parameter Estimation using Permanent Scatterer Interferometry*. PhD thesis. Delft University of Technology. Delft, the Netherlands. PhD thesis.

Kampes, B. M. and Hanssen, R. F. 2004. Ambiguity resolution for permanent scatterer interferometry. *IEEE Transactions on Geoscience and Remote Sensing* 42(11), 2446–2453.

Rodriguez, E. and Martin, J. M. 1992. Theory and design of interferometric synthetic aperture radars. *IEE Proceedings-F* 139(2), 147–159.

Teunissen, P. J. G.: 1994. Least-squares estimation of the integer GPS ambiguities. *Publications and annual report 1993*. number 6 in *LGR-Series*. Delft geodetic computing centre. pp. 59–74.

Teunissen, P. J. G. 1995. The least-squares ambiguity decorellation adjustment: a method for fast GPS integer ambiguity estimation. *Journal of Geodesy* 70(1–2), 65–82.

Teunissen, P. J. G.: 2000a. *Adjustment theory; an introduction*. 1 edn. Delft University Press. Delft.

Teunissen, P. J. G.: 2000b. *Testing theory; an introduction*. 1 edn. Delft University Press. Delft.

Teunissen, P. J. G., de Jonge, P. J. and Tiberius, C. C. J. M. 1995. A new way to fix carrier-phase ambiguities. *GPS World* pp. 58–61.

Verhoef, H. M. E.: 1997. Geodetische deformatie analyse. Lecture notes, Delft University of Technology, Faculty of Geodetic Engineering, in Dutch.